



HAL
open science

Changes in Protein Structure and Distribution Observed at Pre-Clinical Stages of Scrapie Pathogenesis

Ariane Kretlow, Qi Wang, Michael Beekes, Dieter Naumann, Lisa M. Miller

► **To cite this version:**

Ariane Kretlow, Qi Wang, Michael Beekes, Dieter Naumann, Lisa M. Miller. Changes in Protein Structure and Distribution Observed at Pre-Clinical Stages of Scrapie Pathogenesis. *Biochimica et Biophysica Acta - Molecular Basis of Disease*, 2008, 1782 (10), pp.559. 10.1016/j.bbadis.2008.06.004 . hal-00562840

HAL Id: hal-00562840

<https://hal.science/hal-00562840>

Submitted on 4 Feb 2011

HAL is a multi-disciplinary open access archive for the deposit and dissemination of scientific research documents, whether they are published or not. The documents may come from teaching and research institutions in France or abroad, or from public or private research centers.

L'archive ouverte pluridisciplinaire **HAL**, est destinée au dépôt et à la diffusion de documents scientifiques de niveau recherche, publiés ou non, émanant des établissements d'enseignement et de recherche français ou étrangers, des laboratoires publics ou privés.

Accepted Manuscript

Changes in Protein Structure and Distribution Observed at Pre-Clinical Stages of Scrapie Pathogenesis

Ariane Kretlow, Qi Wang, Michael Beekes, Dieter Naumann, Lisa M. Miller

PII: S0925-4439(08)00115-4
DOI: doi: [10.1016/j.bbadis.2008.06.004](https://doi.org/10.1016/j.bbadis.2008.06.004)
Reference: BBADIS 62820

To appear in: *BBA - Molecular Basis of Disease*

Received date: 31 January 2008
Revised date: 2 June 2008
Accepted date: 3 June 2008



Please cite this article as: Ariane Kretlow, Qi Wang, Michael Beekes, Dieter Naumann, Lisa M. Miller, Changes in Protein Structure and Distribution Observed at Pre-Clinical Stages of Scrapie Pathogenesis, *BBA - Molecular Basis of Disease* (2008), doi: [10.1016/j.bbadis.2008.06.004](https://doi.org/10.1016/j.bbadis.2008.06.004)

This is a PDF file of an unedited manuscript that has been accepted for publication. As a service to our customers we are providing this early version of the manuscript. The manuscript will undergo copyediting, typesetting, and review of the resulting proof before it is published in its final form. Please note that during the production process errors may be discovered which could affect the content, and all legal disclaimers that apply to the journal pertain.

Changes in Protein Structure and Distribution Observed at Pre-Clinical Stages of Scrapie Pathogenesis

Ariane Kretlow^{1,2}, Qi Wang², Michael Beekes³, Dieter Naumann¹, and Lisa M. Miller^{2*}

¹P25, Robert Koch-Institut, Nordufer 20, 13353 Berlin, Germany

²National Synchrotron Light Source, Brookhaven National Laboratory, Upton, NY, USA

³ P24, Robert Koch-Institut, Nordufer 20, 13353 Berlin, Germany

*Corresponding author:

Lisa M. Miller, PhD

National Synchrotron Light Source, Bldg 725D

Brookhaven National Laboratory

75 Brookhaven Avenue

Upton, NY 11973

Phone: (631) 344-2091

Fax: (631) 344-3238

Email: lmiller@bnl.gov

Keywords: prion, scrapie, dorsal root ganglia, protein structure, protein-folding, infrared microspectroscopy

Running Title: Protein Structural Changes during Scrapie Pathogenesis

Abbreviations: Transmissible Spongiform Encephalopathy (TSE), dorsal root ganglia (DRG), first clinical signs (fcs), days post infection (dpi), Fourier Transform Infrared Microspectroscopy (FTIRM)

ABSTRACT

Scrapie is a neurodegenerative disorder that involves the misfolding, aggregation and accumulation of the prion protein (PrP). The normal cellular PrP (PrP^C) is rich in α -helical secondary structure, whereas the disease-associated pathogenic form of the protein (PrP^{Sc}) has an anomalously high β -sheet content. In this study, protein structural changes were examined *in situ* in the dorsal root ganglia from perorally 263K scrapie-infected and mock-infected hamsters using synchrotron Fourier Transform InfraRed Microspectroscopy (FTIRM) at four time points over the course of the disease (preclinical, 100 & 130 days post-infection (dpi); first clinical signs (~145 dpi); and terminal (~170 dpi)). Results showed clear changes in the total protein content, structure, and distribution as the disease progressed. At pre-clinical time points, the scrapie-infected animals exhibited a significant increase in protein expression, but the β -sheet protein content was significantly lower than controls. Based on these findings, we suggest that the pre-clinical stages of scrapie are characterized by an overexpression of proteins low in β -sheet content. As the disease progressed, the β -sheet content increased significantly. Immunostaining with a PrP-specific antibody, 3F4, confirmed that this increase was partly – but not solely – due to the formation of PrP^{Sc} in the tissue and indicated that other proteins high in β -sheet were produced, either by overexpression or misfolding. Elevated β -sheet was observed near the cell membrane at pre-clinical time points and also in the cytoplasm of infected neurons at later stages of infection. At the terminal stage of the disease, the protein expression declined significantly, likely due to degeneration and death of neurons. These dramatic changes in protein content and structure, especially at pre-clinical time points, emphasize the possibility for identifying other proteins involved in early pathogenesis, which are important for further understanding the disease.

INTRODUCTION

A characteristic feature of scrapie, a neurodegenerative disorder naturally occurring in sheep and goats, is the accumulation of a β -sheet rich protein termed PrP^{Sc}, or scrapie-associated prion protein, predominantly in the brain and spinal cord. First described in 1732 in sheep, scrapie belongs to the family of Transmissible Spongiform Encephalopathies (TSEs), which can also occur in cattle (bovine spongiform encephalopathy), deer (chronic wasting disease), mink (transmissible mink encephalopathy) and other animals. The Creutzfeldt-Jakob disease in humans can occur sporadically but may also have genetic and infectious origins, which is a unique feature of this group of diseases. According to the prion hypothesis, the causative agent of TSEs is believed to be a proteinaceous infectious particle (“prion”) that lacks agent-specific nucleic acid and consists mainly – if not entirely – of misfolded and pathologically aggregated prion protein [1]. Normal PrP and its pathological isoform have an identical amino acid sequence but different secondary (and tertiary) structures. PrP^C, the cellular prion protein, mainly expressed by neuronal cells, is high in α -helix (42%) and consists of only 3% β -sheet, whereas the misfolded or disease-associated form PrP^{Sc} shows a high amount of β -sheet structure (43%) and has less α -helix (30%) [2].

The nervous system of hamsters orally infected with scrapie has been studied extensively for the temporal-spatial course of PrP^{Sc} deposition (for review see: [3]). After centripetally reaching the spinal cord, subsequent centrifugal spread of PrP^{Sc} deposition proceeds to the corresponding afferent dorsal root ganglia (DRG, nodules on a dorsal spinal root that contain cell bodies of afferent nerve fibers), where the protein can first be detected 76 days post-infection in half of the examined hamsters [4-6]. Immunostained

sections have shown that PrP^{Sc} does not accumulate in all neurons of the DRG, where only certain cells stain strongly. In prion research, conventional techniques like Western Blot analysis are sensitive for examining the total amount of PrP^{Sc} in homogenized tissue. In situ, PET blotting (paraffin embedded tissue blot) [7] labels the misfolded prion protein directly within the tissue, providing spatially-resolved information on the location of PrP^{Sc}. However, both techniques are limited to the detection of PrP^{Sc}, and do not provide information on other compositional changes that occur throughout the disease, especially at early time points in pathogenesis before PrP^{Sc} shows detectable accumulation.

In contrast, Fourier Transform Infrared Microspectroscopy (FTIRM) is an *in situ* technique that is not restricted to the detection of PrP^{Sc}. In fact, an infrared spectrum of a biological sample is composed of characteristic absorption bands that originate from all tissue components, e.g. proteins, lipids, nucleic acids, and carbohydrates. Since the combination of all molecular parameters (structure, composition, and/or interactions) in a specific tissue, cell type, or subcellular component is unique, FTIRM is an *in situ* technique for examining the molecular composition of biological materials [8]. No labels, stains or dyes are required for FTIR microspectroscopy and it is a non-destructive, sensitive and fast analytical tool. Thus, coupled with PrP^{Sc}-specific imaging techniques, FTIRM can be used to determine compositional changes in prion-infected tissue associated with scrapie pathogenesis [9, 10].

In this study, protein content, structure, and distribution throughout scrapie pathogenesis were investigated using synchrotron FTIRM. Syrian hamsters (*Mesocricetus auratus*) perorally infected with scrapie strain 263K were studied at 4

different time points: 100 days post infection (dpi), 130 dpi, at first clinical signs (fcs, ~145 dpi) and at the terminal stage (~170 dpi) of the disease. The total protein, the α -helical protein, and the β -sheet protein contents and distributions were determined as a function of disease progression and correlated with PrP^{Sc} immunostaining. The aim of this study was to examine changes in protein composition throughout scrapie pathogenesis, and to correlate these findings with the temporal-spatial course of PrP^{Sc} deposition. Identification of protein changes involved in early scrapie pathogenesis is important for understanding the disease process and for identifying new approaches for early disease detection and treatment with other, target-oriented techniques.

MATERIALS AND METHODS

Animal experiments and tissue preparation

All animal experiments were carried out in accordance with European, German, and USA legal and ethical regulations. 20 outbred Syrian hamsters at an age of approximately 8 weeks were fed with $1-3 \times 10^7$ 50% intracerebral lethal doses of scrapie strain 263K as described elsewhere [11]. 12 mock-infected hamsters of the same age were similarly fed with normal brain homogenate and served as controls. Five infected and three control hamsters each were euthanized by euthanasia with CO₂, at each of four time points: 100 dpi, 130 dpi, fcs (~145 dpi), and at the terminal stage of the disease (~170 dpi). While the first two time points were fixed dates, fcs and terminal stage depend on the progression of the disease in each individual animal. Fcs is defined as a stage where the animals start to show symptoms that are specific for a 263K scrapie infection in hamsters. These are most commonly a hypersensitivity to touch and noise,

where the animals often twitch, or have difficulties in maintaining balance and rising from a supine position. At the terminal stage, animals show head bobbing, ataxia of gait, and generalized tremor.

After euthanizing the animals, the dorsal root ganglia attached to the thoracic spinal cord were removed and stored at -70°C . After embedding the samples in Jung tissue freezing medium (Leica Instruments, Germany), $10\ \mu\text{m}$ thick cryo-sections were cut at a temperature of -20°C and mounted on IR transparent slides (CaF_2 , 1 mm in thickness) (Korth Kristalle GmbH, Altenholz, Germany). Adjacent sections were cut at the same thickness and mounted on standard glass microscope slides for immunostaining. The CaF_2 slides were kept in a dry and dark environment until the FTIR microspectroscopic measurements were carried out. One animal died before reaching the stage of fcs, resulting in a total of 19 infected and 12 mock-infected control animals included in the study.

Immunohistochemistry

Adjacent sections on glass slides were stained for PrP using the monoclonal antibody 3F4 as described previously [12]. In short, the slides were fixed three times: 5 min each in 50, 100 and 50% ethanol, and then rehydrated in distilled water. The ganglia were then treated with 10% phosphate buffered formalin for 15 min, 100 mM NH_4Cl and 0.5% Igepal in PBS (pH 7.8) for 5 min each. Sections were denatured in 3M Guanidiniumthiocyanate/10 mM TrisHCl (pH 7.8). They were blocked overnight with fetal calf serum in TBST/0.2% Tween 20 at 4°C , incubated with antibody 3F4 (1:100) for 1 h 45 min and then with biotinylated secondary antibody Goat-anti-Mouse (Dako E 0433) (1:200) in PBS/1%BSA. Finally the sections were incubated with Vectastain ABC

Kit and stained with preincubation and incubation solution containing 3,3-Diaminobenzidin (DAB) to visualize the reaction product for 10 min and 3 min, respectively. For negative controls, ganglia slices were incubated in normal mouse serum (Dako) (1:1000) instead of mAb 3F4 prior to incubation with the secondary antibody. After FTIRM data collection, the ganglia on CaF₂ windows were also immunostained accordingly.

FTIRM Data collection

The FTIRM experiments were conducted at beamline U10B at the National Synchrotron Light Source, Brookhaven National Laboratory (Upton, NY). A Thermo Nicolet Magna 860 FTIR spectrometer, coupled to a Continuum FTIR microscope (ThermoNicolet, Madison, WI), was used with synchrotron light as the infrared source. The microscope was equipped with matching 32X Schwarzschild objectives, a motorized x-y mapping stage, an adjustable rectangular aperture, and a mercury cadmium telluride (MCT-A) detector. The aperture of the microscope was set to 10 x 10 μm . A pre-defined area of approximately 100 x 100 μm encompassing about 15 - 20 cells was raster-scanned with a step size of 4 μm using Omnic software (ThermoNicolet). At each point, an absorbance spectrum was recorded in transmission mode. Each spectrum was collected in the mid-infrared spectral range (800 - 4000 cm^{-1}) with a spectral resolution of 8 cm^{-1} and 128 scans co-added. Happ-Genzel apodization and a zero-filling of level 2 were applied, resulting in approximately 1 data point per wavenumber. A background spectrum on clean substrate was also recorded by co-adding 512 scans. For each animal, one or two infrared maps were collected, yielding an average of 10500 spectra from 138

cells (~29 cells per animal) per time point from the infected animals and 8887 spectra from 110 cells (~37 cells per animal) per time point from the controls.

Data Analysis

The FTIRM data were analyzed using Thermo Nicolet's software Omnic 7.3. Absorbances from 1616 to 1636 cm^{-1} of protein infrared spectra are attributed primarily to β -sheet structures, which have been shown to increase in studies of recombinant and protease-resistant Syrian hamster PrP in vitro [13-16]. Thus, to examine the relative content of β -sheet structure in the tissue, each absorbance spectrum was integrated from 1624 - 1628 cm^{-1} , applying a linear baseline from 1480 – 1715 cm^{-1} . To normalize for potential differences in tissue thickness among samples, the β -sheet area was divided by the area under the Amide I protein band (1600 – 1700 cm^{-1}), applying the same linear baseline. Accordingly, the relative α -helical content was calculated by integrating each absorbance spectrum from 1654 – 1658 cm^{-1} and normalizing to the area under the Amide I band. For both α -helix and β -sheet content, narrow regions were integrated in order to prevent overlap with other secondary structure elements [17]. Chemical images in α -helix and β -sheet content were generated using Transform (Fortner Software, USA). To estimate the relative protein content at each pixel, the integrated area under the Amide I protein band was divided by the area under the entire infrared spectrum, in order to normalize for potential differences in tissue thickness among samples. The total integrated area was calculated as the integrated area from 2500 - 3700 cm^{-1} (baseline from 2500 to 3700 cm^{-1}) plus the integrated area from 1760 – 1000 cm^{-1} (baseline from 1760 – 1000 cm^{-1}). The whole spectral region was chosen since it includes the vibrational modes of C-H, N-H and O-H bonds of all major biomolecules and therefore

represents the total biomass. Thus, by dividing the total protein by the total biomass, a relative estimate of total protein content was determined.

For each animal, the α -helix, β -sheet, and total protein content were determined for every pixel in each map. These values were averaged to obtain a mean and standard deviation for each animal. Then the individual animal values were averaged at their respective time points. An unpaired, two-sided t-test (Student's t-test) was performed on all data to test for significant differences ($p < 0.05$) between scrapie and control at each time point, and differences between time points. In the analysis, those spectra derived from areas outside the ganglion or from tissue artifacts were excluded from the calculation.

RESULTS

To examine changes in the secondary structure of proteins as a function of disease severity, the mean values \pm standard deviation for β -sheet content were calculated and plotted in **Figure 1A**. As disease progressed, results showed that the amount of β -sheet remained relatively constant in control hamsters (gray line), but substantially increased with time in the scrapie-infected animals (black line). The most dramatic difference between the control and infected animals was observed at 100 dpi, where the β -sheet content in scrapie-infected ganglia was significantly lower than in the control ganglia ($p = 0.013$). Over the course of the disease, we found a significant increase in β -sheet content in the infected animals of about 8% ($p = 0.003$). In contrast, the β -sheet content in the control ganglia remained unchanged over the time course studied here.

In contrast to the dramatic changes in β -sheet, **Figure 1B** shows that the α -helical content was unaffected by the disease (black line) or by age (control, gray line).

To determine how the changes in protein structure were related to total protein expression, the total protein content was determined as a function of disease severity (**Figure 1C**). At 100 dpi, the scrapie-infected animals (black line) showed a significant increase in relative protein content when compared to the control animals ($p=0.020$). Moreover, the total protein content of scrapie-infected animals (black line) declined gradually during pathogenesis and reached a significantly lower level at the terminal stage of the disease ($p=0.013$). The control animals did not exhibit a change in total protein expression throughout the time course studied here.

In addition to measuring relative protein content and structure, the spatial distribution of β -sheet protein within the tissue was also examined. In **Figure 2**, photomicrographs and corresponding FTIRM images of the intermolecular β -sheet distribution for representative control (left) and infected (right) ganglia at different time points are shown. In all images, the β -sheet content was slightly higher near the cell's periphery and extracellular matrix. For the control animals, the FTIRM images appeared similar at each time point, indicating that the β -sheet distribution remained constant over time. For the scrapie-infected animals, it can be seen that the β -sheet content increases with the progression of the disease, as indicated by more green, yellow, and red areas. At pre-clinical time points, elevated β -sheet was detected in only a few cells and exclusively near the cell membrane. Otherwise, these cells generally exhibited proteins lower in β -sheet content than the controls, as can be seen by the dark blue areas. During disease progression, the number of affected cells increased such that, by the terminal stage,

overall content of β -sheet increased and was observed throughout a large number of cells, including – but not limited to – the cell's periphery.

To further investigate the distribution of α -helix, β -sheet, and unordered structures in scrapie-infected tissue, second derivative spectra from a 100 dpi scrapie-infected animal are plotted in **Figure 3**. These spectra were obtained from the regions marked with asterisks in **Figure 2** (scrapie, 100 dpi panel). In most cells at 100 dpi, the typical FTIR spectrum is primarily α -helical, with an intense absorption feature at 1656 cm^{-1} (obtained from points in the center of the cell indicated by white asterisk in **Figure 2**.) However, the area near the cell membrane (black asterisk in **Figure 2**) exhibited spectra with increased peak intensities at 1681 cm^{-1} (attributed to β -turns and loops), 1638 and 1632 cm^{-1} (attributed to β -sheet), and a broad shoulder at around 1648 cm^{-1} (attributed to unordered structures), while the intensity of the α -helical peak at around 1656 cm^{-1} was shown to decrease slightly [16], indicating changes in a number of secondary structures, beyond α -helix and β -sheet.

Since the FTIRM data showed an increase in β -sheet content with disease progression, consistent with the accumulation of PrP^{Sc} , immunostaining with the 3F4 antibody for the prion protein was performed on adjacent tissue sections (**Figure 4**). Due to the fact that the antibody 3F4 stains both the cellular and the misfolded form of the prion protein [18], a more or less homogeneous brown background can be seen in all images, where the intensity or distribution does not significantly change between time points or infection state. However, in the infected tissue, comparative immunohistochemical and PET blot staining has shown that PrP^{Sc} accumulates as micro disperse aggregates that present as characteristic granular deposits of immunoreactive

material [5]. **Figure 4** shows a clear progression of PrP^{Sc} deposition during pathogenesis by the increased appearance of brown, granular, immunoreactive material, indicating the presence of pathologically aggregated PrP. At 100 dpi, very few neurons and satellite cells showed such immunostaining for PrP^{Sc}, whereas the accumulation of PrP^{Sc} became more prominent at later stages of incubation as indicated by the increasing number of characteristic granular deposits at 130 dpi, fcs, and at the terminal stage of disease.

To directly correlate the elevated β -sheet content with the distribution of aggregated PrP^{Sc}, the FTIRM samples were subsequently stained with the 3F4 monoclonal antibody. **Figure 5** shows the results for an infected animal at 100 dpi (left column) and at first clinical signs (right column). The first row displays the unstained photomicrographs, while the second row shows the same tissue stained with the 3F4 antibody. At 100 dpi, the immunostained section shows no evidence of PrP^{Sc} inside the neurons, but in some of the surrounding satellite cells (arrows). The third and fourth rows represent the β -sheet and α -helix distributions, respectively, as measured with FTIRM. At 100 dpi, the satellite cells that stained positive for PrP^{Sc} also have higher β -sheet content. Furthermore, some areas showed both elevated β -sheet and α -helical content (asterisks). At fcs, some neurons stained positive for PrP^{Sc} (as can be seen by granular deposits and indicated by arrows) and show a high content of β -sheet in the corresponding FTIRM map (e.g. the cell in the center of the image). In contrast, the cell shown in the upper left of the fcs photomicrograph (arrowhead) shows elevated β -sheet content but no PrP^{Sc} staining, indicating that β -sheet rich proteins other than PrP^{Sc} also increase during pathogenesis.

DISCUSSION

FTIR spectra of isolated PrP fragments (PrP₂₇₋₃₀) and protease-resistant PrP (PrP^{res}) from 263K scrapie infected hamster were shown to exhibit strong absorbance bands at around 1636 and 1626 cm⁻¹, indicating the presence of β -sheet structures [13, 14, 16]. Furthermore, under destabilizing conditions and low pH, recombinant Syrian hamster prion protein showed dominant amide I band components at 1620 and 1691 cm⁻¹, which are generally assigned to intermolecularly arranged antiparallel β -sheet structures [15]. Site-directed spin labeling, EPR spectroscopy, and time resolved FTIR studies revealed that the conformational conversion of PrP^C into PrP^{Sc} involves major refolding of the C-terminal α -helical region of PrP^C [19, 20]. But not all α -helices get converted into β -sheet, as was shown by NMR [21]. However, while FTIR spectroscopy has been able to identify structural changes in PrP *in vitro* and *ex situ*, identification of structural changes within scrapie-infected tissue has been difficult.

Recently, a FTIRM study of terminally-diseased, 263K scrapie hamsters was the first to show a higher β -sheet content and a lower α -helical content in infected DRG cells [22, 23]. Here, this study has been extended to pre-clinical time points, and we find significant changes in protein structure, composition, and distribution throughout the course of the disease, while age-matched control animals did not exhibit any changes over the investigated time period. Specifically, we find that elevated β -sheet content was detectable earlier in the disease, i.e. with the onset of the first clinical signs. These findings are consistent with work by McBride, et al., who used immunostaining to show PrP^{Sc} accumulation as early as 76 days post infection in the 263K scrapie hamster model [5].

Over the course of the disease, results show that the increase in β -sheet was $\sim 8\%$, well above the amount attributable to PrP^{Sc} , which was shown to represent only 0.1% of all proteins in the tissue at terminal stage [24]. Furthermore, FTIRM and corresponding immunostain images revealed that not all areas with elevated β -sheet stained positive for PrP^{Sc} , indicating that other β -sheet rich proteins also play a role in scrapie pathogenesis. Gene profiling of 263K scrapie infected hamster identified several upregulated genes at the terminal time point [25, 26]. Among those were proteins with predominantly β -sheet content, such as metallothionein [27], apolipoprotein J [28], IP-10 [29, 30] and β_2 -microglobulin, the last of which was shown to have amyloidogenic properties [31]. However, since FTIRM spectra represent the average protein structure within the volume of tissue illuminated by the infrared light, specific identification of these proteins is beyond the scope of this study.

While an increase in β -sheet content towards the terminal stage of the disease confirmed our initially proposed hypothesis, a significantly lower amount of β -sheet protein at pre-clinical time points was an unexpected finding. Since the total protein content was significantly increased in the scrapie-infected animals at 100 dpi, we suggest that the early scrapie infection is characterized by an overexpression of proteins low in β -sheet content. Second derivative analysis confirmed that most spectra showed predominantly high α -helical content; however some spectra recorded near the cell's periphery exhibited an increase in random coil and β -sheet content. Immunohistochemistry studies have previously shown that the deposition of pathological PrP^{Sc} starts in satellite cells and in the cytoplasm and plasmalemma of neurons [6]. PrP^{Sc} accumulation near the cell membrane has also been observed in scrapie-infected mouse

neuroblastoma cells [32], in cultured Chinese hamster ovary cells [33], in the medulla oblongata, pons, and astrocytes of sheep [34], and mice with natural scrapie [35, 36].

At later stages of pathogenesis, the β -sheet content increased throughout the cell, which is consistent with (but not exclusively attributed to) the appearance of PrP^{Sc} aggregates in the cytoplasm of neurons, primarily in secondary lysosomes [37], agrosomes [38], and in the nucleus [39]. Interestingly, accumulation of PrP in the cytosol has been shown to be neurotoxic [40, 41].

In summary, this study showed that pronounced protein-related changes occur at the very early stages of scrapie pathogenesis, well before clinical symptoms appear. Moreover, these changes go well beyond the transformation of PrP^C to PrP^{Sc}. In the future, efforts to identify these specific proteins that are involved at pre-clinical time points may provide an avenue for early disease detection and possible targets for treatment of scrapie infection that are not available today.

ACKNOWLEDGEMENTS

The authors like to thank Marion Joncic and Kristin Kampf (Robert Koch-Institute) for skillful technical assistance with the animal experiments. We are also grateful to the technical and safety staff at the NSLS, especially to Randy Smith, Larry Carr, and Andrew Ackerman. M. B. is grateful for ongoing support by the EU-funded Network of Excellence “NeuroPrion”. This work was funded by the National Institutes of Health Grant R01-GM66873. The National Synchrotron Light Source is funded by the U.S. Department of Energy, Office of Science, Office of Basic Energy Sciences, under Contract No. DE-AC02-98CH10886.

REFERENCES

- [1] S.B. Prusiner. Prion diseases and the BSE crisis, *Science* 278 (1997) 245-51.
- [2] K.M. Pan, M. Baldwin, J. Nguyen, M. Gasset, A. Serban, D. Groth, I. Mehlhorn, Z. Huang, R.J. Fletterick, F.E. Cohen and et al. Conversion of alpha-helices into beta-sheets features in the formation of the scrapie prion proteins, *Proc Natl Acad Sci U S A* 90 (1993) 10962-6.
- [3] M. Beekes and P.A. McBride. The spread of prions through the body in naturally acquired transmissible spongiform encephalopathies, *Febs J* 274 (2007) 588-605.
- [4] M. Beekes, P.A. McBride and E. Baldauf. Cerebral targeting indicates vagal spread of infection in hamsters fed with scrapie, *J Gen Virol* 79 (Pt 3) (1998) 601-7.
- [5] P.A. McBride, W.J. Schulz-Schaeffer, M. Donaldson, M. Bruce, H. Diringer, H.A. Kretzschmar and M. Beekes. Early spread of scrapie from the gastrointestinal tract to the central nervous system involves autonomic fibers of the splanchnic and vagus nerves, *J Virol* 75 (2001) 9320-7.
- [6] P.A. McBride and M. Beekes. Pathological PrP is abundant in sympathetic and sensory ganglia of hamsters fed with scrapie, *Neurosci Lett* 265 (1999) 135-8.
- [7] W.J. Schulz-Schaeffer, S. Tschoke, N. Kranefuss, W. Drose, D. Hause-Reitner, A. Giese, M.H. Groschup and H.A. Kretzschmar. The paraffin-embedded tissue blot detects PrP(Sc) early in the incubation time in prion diseases, *Am J Pathol* 156 (2000) 51-6.

- [8] D.L. Wetzel and S.M. LeVine. Imaging molecular chemistry with infrared microscopy, *Science* 285 (1999) 1224-5.
- [9] J. Kneipp, M. Beekes, P. Lasch and D. Naumann. Molecular changes of preclinical scrapie can be detected by infrared spectroscopy, *J Neurosci* 22 (2002) 2989-97.
- [10] J. Kneipp, P. Lasch, E. Baldauf, M. Beekes and D. Naumann. Detection of pathological molecular alterations in scrapie-infected hamster brain by Fourier transform infrared (FT-IR) spectroscopy, *Biochim Biophys Acta* 1501 (2000) 189-99.
- [11] E. Baldauf, M. Beekes and H. Diringer. Evidence for an alternative direct route of access for the scrapie agent to the brain bypassing the spinal cord, *J Gen Virol* 78 (Pt 5) (1997) 1187-97.
- [12] Q. Wang, A. Kretlow, M. Beekes, D. Naumann and L. Miller. In situ characterization of prion protein structure and metal accumulation in Scrapie-Infected Cells by Synchrotron Infrared and X-ray Imaging, *Vibrational Spectroscopy* 38 (2005) 61-69.
- [13] A. Troullier, D. Reinstadler, Y. Dupont, D. Naumann and V. Forge. Transient non-native secondary structures during the refolding of alpha-lactalbumin detected by infrared spectroscopy, *Nat Struct Biol* 7 (2000) 78-86.
- [14] B. Caughey, G.J. Raymond and R.A. Bessen. Strain-dependent differences in beta-sheet conformations of abnormal prion protein, *J Biol Chem* 273 (1998) 32230-5.

- [15] F. Sokolowski, A.J. Modler, R. Masuch, D. Zirwer, M. Baier, G. Lutsch, D.A. Moss, K. Gast and D. Naumann. Formation of critical oligomers is a key event during conformational transition of recombinant syrian hamster prion protein, *J Biol Chem* 278 (2003) 40481-92.
- [16] S. Spassov, M. Beekes and D. Naumann. Structural differences between TSEs strains investigated by FT-IR spectroscopy, *Biochim Biophys Acta* 1760 (2006) 1138-49.
- [17] H. Fabian and D. Naumann. Methods to study protein folding by stopped-flow FT-IR, *Methods* 34 (2004) 28-40.
- [18] R.J. Kascsak, R. Rubenstein, P.A. Merz, M. Tonna-DeMasi, R. Fersko, R.I. Carp, H.M. Wisniewski and H. Diringer. Mouse polyclonal and monoclonal antibody to scrapie-associated fibril proteins, *Journal of virology* 61 (1987) 3688-93.
- [19] N.J. Cobb, F.D. Sonnichsen, H. McHaourab and W.K. Surewicz. Molecular architecture of human prion protein amyloid: a parallel, in-register beta-structure, *Proc Natl Acad Sci U S A* 104 (2007) 18946-51.
- [20] J. Ollesch, E. Kunnemann, R. Glockshuber and K. Gerwert. Prion protein alpha-to-beta transition monitored by time-resolved Fourier transform infrared spectroscopy, *Appl Spectrosc* 61 (2007) 1025-31.
- [21] J. Watzlawik, L. Skora, D. Frense, C. Griesinger, M. Zweckstetter, W.J. Schulz-Schaeffer and M.L. Kramer. Prion protein helix1 promotes aggregation but is not converted into beta-sheet, *J Biol Chem* 281 (2006) 30242-50.

- [22] J. Kneipp, L.M. Miller, M. Joncic, M. Kittel, P. Lasch, M. Beekes and D. Naumann. In situ identification of protein structural changes in prion-infected tissue, *Biochim Biophys Acta* 1639 (2003) 152-8.
- [23] J. Kneipp, L.M. Miller, S. Spassov, F. Sokolowski, P. Lasch, M. Beekes and D. Naumann. Scrapie-infected cells, isolated prions, and recombinant prion protein: a comparative study, *Biopolymers* 74 (2004) 163-7.
- [24] M. Beekes, E. Baldauf, S. Cassens, H. Diringer, P. Keyes, A.C. Scott, G.A. Wells, P. Brown, C.J. Gibbs, Jr. and D.C. Gajdusek. Western blot mapping of disease-specific amyloid in various animal species and humans with transmissible spongiform encephalopathies using a high-yield purification method, *J Gen Virol* 76 (Pt 10) (1995) 2567-76.
- [25] C. Riemer, I. Queck, D. Simon, R. Kurth and M. Baier. Identification of upregulated genes in scrapie-infected brain tissue, *J Virol* 74 (2000) 10245-8.
- [26] M.J. Stobart, D. Parchaliuk, S.L. Simon, J. Lemaistre, J. Lazar, R. Rubenstein and J.D. Knox. Differential expression of interferon responsive genes in rodent models of transmissible spongiform encephalopathy disease, *Mol Neurodegener* 2 (2007) 5.
- [27] Y. Boulanger, C.M. Goodman, C.P. Forte, S.W. Fesik and I.M. Armitage. Model for mammalian metallothionein structure, *Proc Natl Acad Sci U S A* 80 (1983) 1501-5.
- [28] M. Calero, T. Tokuda, A. Rostagno, A. Kumar, B. Zlokovic, B. Frangione and J. Ghiso. Functional and structural properties of lipid-associated apolipoprotein J (clusterin), *Biochem J* 344 Pt 2 (1999) 375-83.

- [29] V. Booth, D.W. Keizer, M.B. Kamphuis, I. Clark-Lewis and B.D. Sykes. The CXCR3 binding chemokine IP-10/CXCL10: structure and receptor interactions, *Biochemistry* 41 (2002) 10418-25.
- [30] G.J. Swaminathan, D.E. Holloway, R.A. Colvin, G.K. Campanella, A.C. Papageorgiou, A.D. Luster and K.R. Acharya. Crystal structures of oligomeric forms of the IP-10/CXCL10 chemokine, *Structure* 11 (2003) 521-32.
- [31] Z. Zhang, H. Chen and L. Lai. Identification of amyloid fibril-forming segments based on structure and residue-based statistical potential, *Bioinformatics* 23 (2007) 2218-25.
- [32] B. Caughey and G.J. Raymond. The scrapie-associated form of PrP is made from a cell surface precursor that is both protease- and phospholipase-sensitive, *The Journal of Biological Chemistry* 266 (1991) 18217-23.
- [33] S. Lehmann and D.A. Harris. Mutant and infectious prion proteins display common biochemical properties in cultured cells, *The Journal of biological chemistry* 271 (1996) 1633-7.
- [34] L.J. van Keulen, B.E. Schreuder, R.H. Melen, M. Poelen-van den Berg, G. Mooij-Harkes, M.E. Vromans and J.P. Langeveld. Immunohistochemical detection and localization of prion protein in brain tissue of sheep with natural scrapie, *Vet Pathol* 32 (1995) 299-308.
- [35] M. Jeffrey, C.M. Goodsir, M.E. Bruce, P.A. McBride, N. Fowler and J.R. Scott. Murine scrapie-infected neurons in vivo release excess prion protein into the extracellular space, *Neurosci Lett* 174 (1994) 39-42.

- [36] M. Jeffrey, C.M. Goodsir, M.E. Bruce, P.A. McBride and J.R. Scott. Infection-specific prion protein (PrP) accumulates on neuronal plasmalemma in scrapie-infected mice, *Ann N Y Acad Sci* 724 (1994) 327-30.
- [37] M. Jeffrey, G. McGovern, C.M. Goodsir, K.L. Brown and M.E. Bruce. Sites of prion protein accumulation in scrapie-infected mouse spleen revealed by immunoelectron microscopy, *J Pathol* 191 (2000) 323-32.
- [38] E. Cohen and A. Taraboulos. Scrapie-like prion protein accumulates in aggresomes of cyclosporin A-treated cells, *Embo J* 22 (2003) 404-17.
- [39] A. Mange, C. Crozet, S. Lehmann and F. Beranger. Scrapie-like prion protein is translocated to the nuclei of infected cells independently of proteasome inhibition and interacts with chromatin, *J Cell Sci* 117 (2004) 2411-6.
- [40] J. Ma, R. Wollmann and S. Lindquist. Neurotoxicity and neurodegeneration when PrP accumulates in the cytosol, *Science* 298 (2002) 1781-5.
- [41] A.S. Rambold, M. Miesbauer, D. Rapaport, T. Bartke, M. Baier, K.F. Winklhofer and J. Tatzelt. Association of Bcl-2 with misfolded prion protein is linked to the toxic potential of cytosolic PrP, *Mol Biol Cell* 17 (2006) 3356-68.

FIGURE CAPTIONS

Figure 1: Mean values \pm average deviation for the relative (A) β -sheet protein content, (B) α -helix protein content, and (C) total protein content for scrapie-infected (black lines) and control (white lines) hamster dorsal root ganglia at the four investigated time points. Asterisks mark significant differences ($p < 0.05$) between scrapie and control.

Figure 2: (A) Photomicrographs of unstained cryosections (1st and 3rd column) and corresponding FTIRM images (2nd and 4th column) of the β -sheet distribution for control (left) and infected (right) ganglia at different time points. Scale bar: 20 μm .

Figure 3: Original and second derivative spectra derived from near the cell membrane (black line) and within the cytoplasm (gray line) of a 100 dpi scrapie-infected animal.

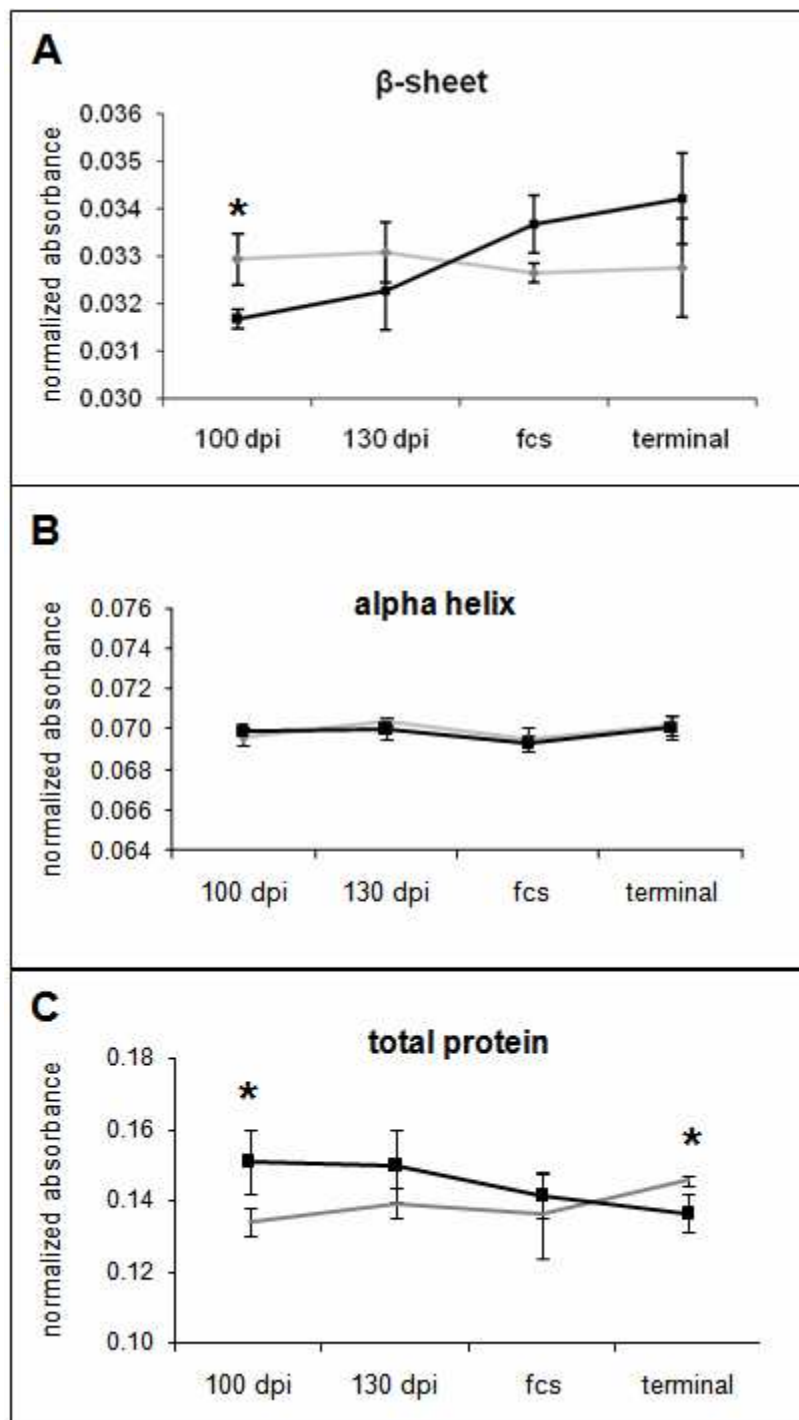
Figure 4: Photomicrographs of antibody 3F4-stained adjacent sections. PrP^{Sc} can be detected as granular deposits of immunoreactive material (arrows) in many – but not all – of the neuronal and satellite cells at later stages of incubation. Scale bar: 30 μm .

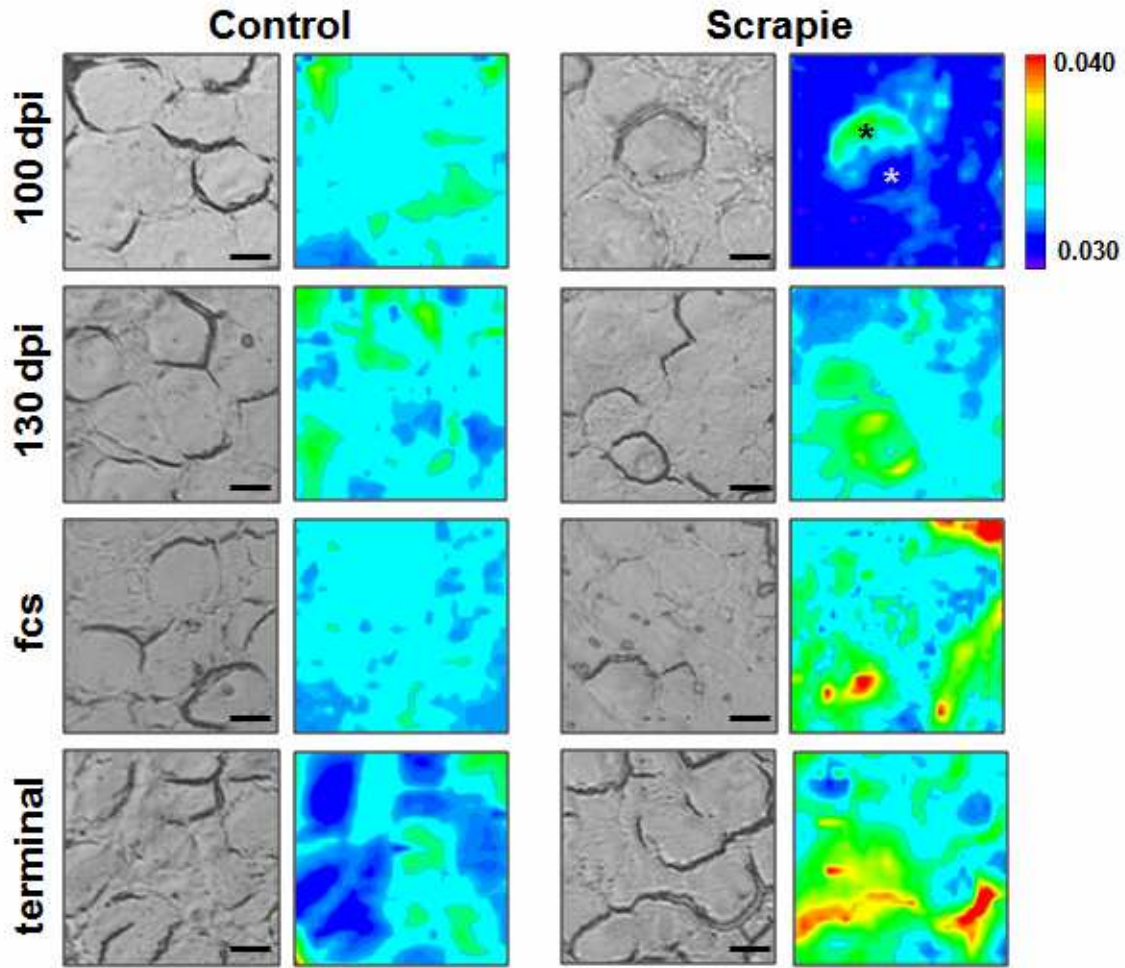
Figure 5: Comparison of the results from the FTIRM of an infected animal at 100 dpi (left) and first clinical signs (right) with 3F4-stained sections of the same tissue. Photomicrographs of the areas investigated with FTIRM are shown in the 1st row (unstained) and 2nd row (3F4-antibody stained). The β -sheet and α -helix distributions are represented in the 3rd and 4th rows, respectively. At 100 dpi, some areas show high β -

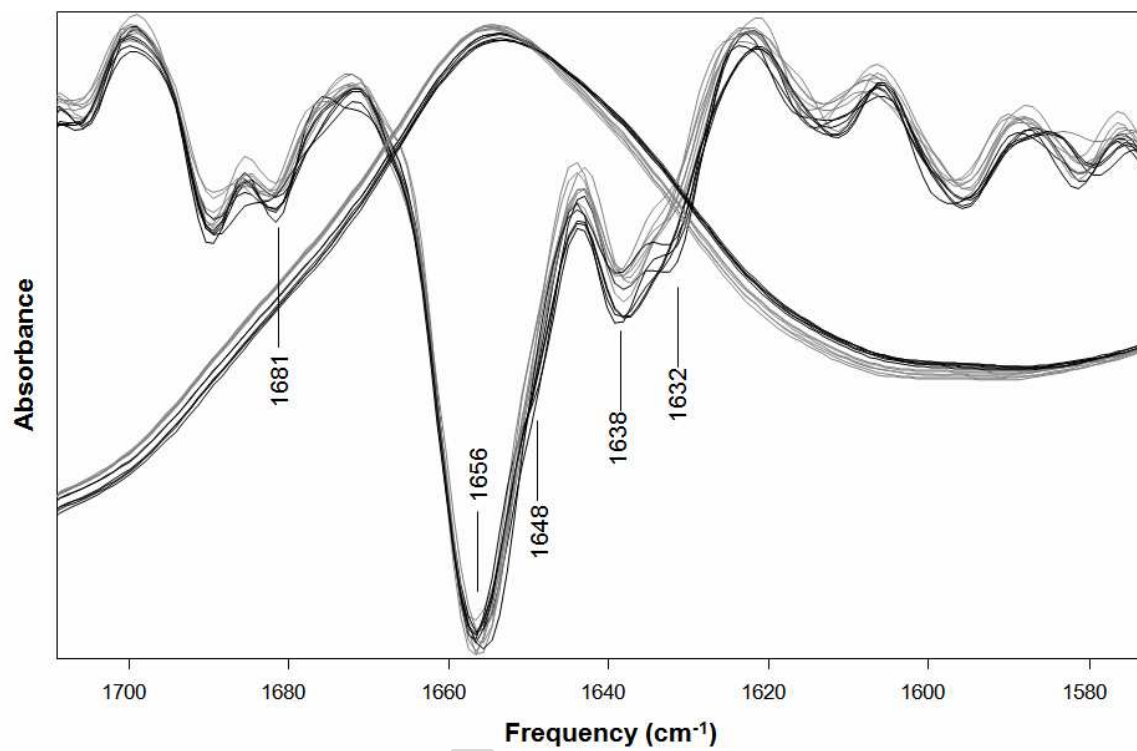
sheet as well as high α -helix (*), which was not observed at the terminal stage. Areas with PrP^{Sc} deposition as seen in the 3F4 stained sections showed elevated β -sheet (arrows), while some areas showed high β -sheet but no PrP^{Sc} deposition (arrowheads).

Scale bar: 20 μ m.

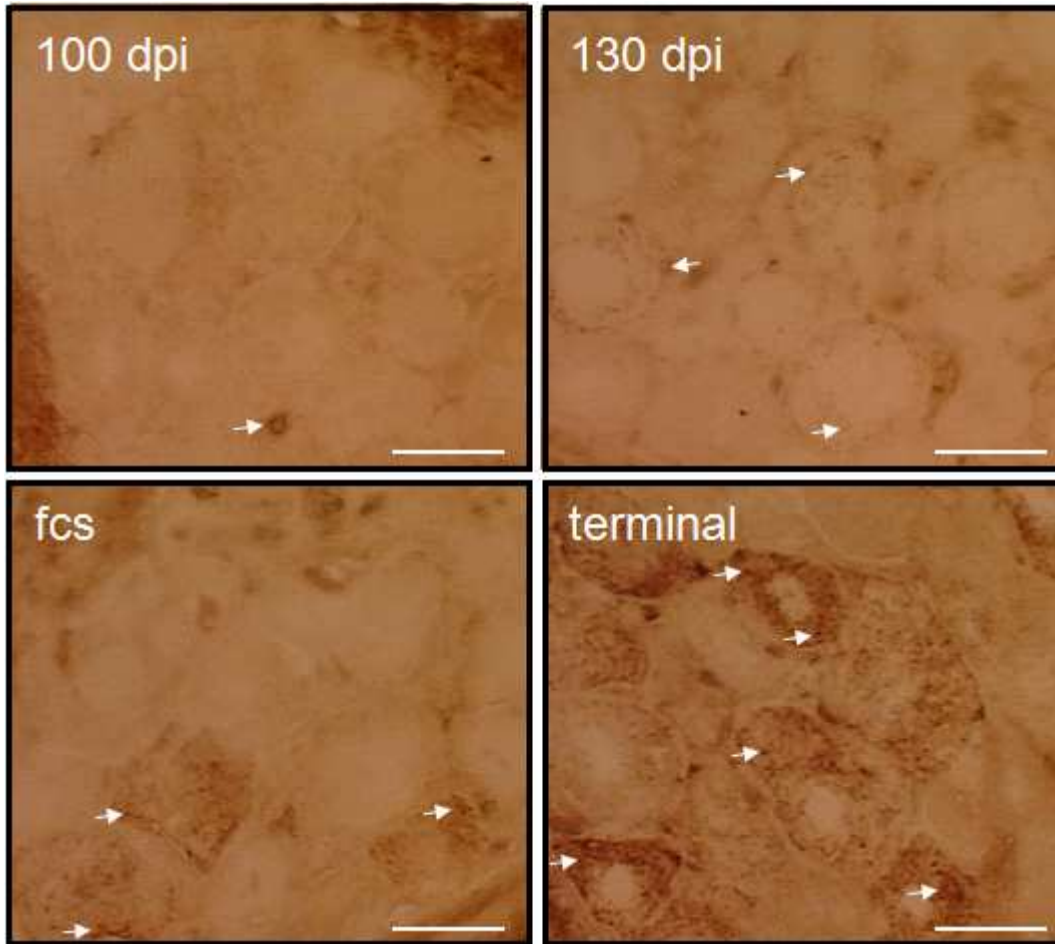
ACCEPTED MANUSCRIPT







ACCEPTED



ACCEPTED

